Determination of Soil Properties Utilizing C-Band Synthetic Aperture Radar (SAR) in Southern Kirkuk Governate, Northern Iraq

Birjan Qasim Shakir
Department of Surveying Engineering Techniques, Technical Engineering College-Kirkuk, Northern Technical University, Mosul, Iraq
birjan.qasimgs@ntu.edu.iq (corresponding author)

Muntadher Aidi Shareef
Department of Surveying Engineering Techniques, Technical Engineering College-Kirkuk, Northern Technical University, Mosul, Iraq
muntadher.a.shareef@ntu.edu.iq

Qahtan A. M. Al Nuaimy
Department of Surveying Engineering Techniques, Technical Engineering College-Kirkuk, Northern Technical University, Mosul, Iraq
qahtaniraqi@ntu.edu.iq

Received: 16 May 2025 | Revised: 2 June 2025 | Accepted: 8 June 2025

 DOI: https://doi.org/10.48084/etasr.12189

ABSTRACT

This study utilizes Synthetic Aperture Radar (SAR) images to assess and monitor the soil properties. To achieve this, it provides an efficient method for soil resource evaluation in the designated area to increase the information accessibility and minimize the costs and efforts. Sentinel-1 C-SAR images (VV, VH), were collected on 6-Oct-2024 in Taza Khurmatu district, southern Kirkuk, Northern Iraq, which were used as ancillary data. Sentinel-1 C-SAR was joined with field-soil data and machine learning was utilized to classify different kinds of soil properties. The effectiveness of SAR data to predict the soil texture, salt content, and organic properties was confirmed. With this technique, significantly less in-field sampling is required, while it is cost-effective and flexible. Its novelty lies in the discovery that radar data closely correlate with the soil characteristics in a region where this relationship had not previously been explored. Several soil parameters were examined and correlated during the study. These parameters include, texture, organic matter content, salinity, pH, and lime content. The former directly influence the SAR backscatter. The results showed that the study area consists of fine materials where silt appears most frequently, followed by clay, while the sand and gravel contents are minimal. The soil characteristics indicate effective moisture retention, but the sand portion needs evaluation, regarding the drainage performance. However, a medium to low level of plasticity was observed from the plastic and liquid limits. The multiple linear regression analysis revealed strong correlations between the calculated regression coefficients, which ranged from 0.590 to 0.930, and the recorded chemical and physical data. A Unified Soil Classification System (USCS) identified eight soil types throughout the region based on the clay, silt, sand, and gravel content. In addition, C-band radar data were effectively used to predict other soil properties through the K-Dimensional Tree (KD-Tree), K-Nearest Neighbor (KNN), Random Forest (RF), and Minimum Distance (MD) classifiers. The study findings demonstrate that field-based algorithm classification methods can be created from C-band SAR observations. However, this method's suitability for different geographic areas remains untested.

Keywords-soil texture; Synthetic Aperture Radar (SAR); backscatter; Sentinel-1; Random Forest (RF)

I. INTRODUCTION

The soil is an important natural resource, providing an essential and diversified natural platform for all terrestrial life [1]. It is also defined in engineering applications as the unconsolidated assemblage of mineral grains and decomposed organic matter (solid particles) containing liquid and gas in the pore space between the solid particles [2, 3]. Monitoring the soil characteristics is essential for efficient soil management [4,

5]. It has been also shown that GIS is an ideal solution for engineering applications with a particular emphasis on pathfinding and site selection [6, 7]. This technique provides fast measurements of the soil characteristics [1] for a detailed spatial analysis across extensive geographic areas [8].

Furthermore, SAR is an active microwave remote sensing system used for Earth observation. SAR image radiometry, including backscatter coefficient estimation and reflectance measurement, requires specific methodologies depending on the type of satellite data used [9]. To achieve successful calibration, each satellite needs customized procedures based on its operational requirements [10]. Regression analysis is conducted to ascertain the correlations between two or more variables exhibiting cause-and-effect relationships and to facilitate the predictions about the subject based on these relationships [11, 12]. The soil texture significantly varies based on the type and amount of clay minerals present [13]. However, the soil quality evaluation requires more than simply measuring the soil moisture, since the soil consists of a dynamic and complex structure depending on multiple interactions [5, 14, 15]. In this regard, the soil characteristic predictions across terrains have completely changed [16] owing to the GIS and modeling techniques [17].

This study employs an efficient approach to soil resource assessment by integrating parametric evaluation with textural analysis of radar imagery. To achieve this objective, various techniques, such as KNN, KD-Tree, RF, and MD were employed, while the accuracy verification was performed using the SNAP 11 software. Satellite data were collected from European Space Agency (ESA). Multiple linear regressions for data analysis were performed through the use of the SPSS 26 software. The GIS 10.8 software helped in establishing the sand-silt-clay composition ratios in the soil samples.

II. STUDY AREA

The study area is located in Taza Khurmatu district, approximately 10 km from Kirkuk and 230 km from Baghdad, Iraq. The latitude and longitude lines defining the study area range from 3904000 to 3910000 N, and 437000 to 441000 E, as shown in Figure 1. It is located in a low folded area in the Makhoul-Hamrin tectonic subzone in Iraq and within the alluvial fan deposits, which are preserved in various locations around the region under study [18].

III. MATERIALS AND METHODS

Figure 2 illustrates the procedures and steps followed in this study, including the field and laboratory data collection, along with the use of satellite data.

A. Field Data

To determine the moisture content and dry density, 1.5-2 kg of soil samples was collected from a surface of about 10-20 cm depth. Other samples were collected from greater depths (20-30 cm) to evaluate the physical and chemical properties of the selected locations. The measurements of the soil moisture and dry density were conducted in the field via the moisture and density gauges (HS-5001EZ).

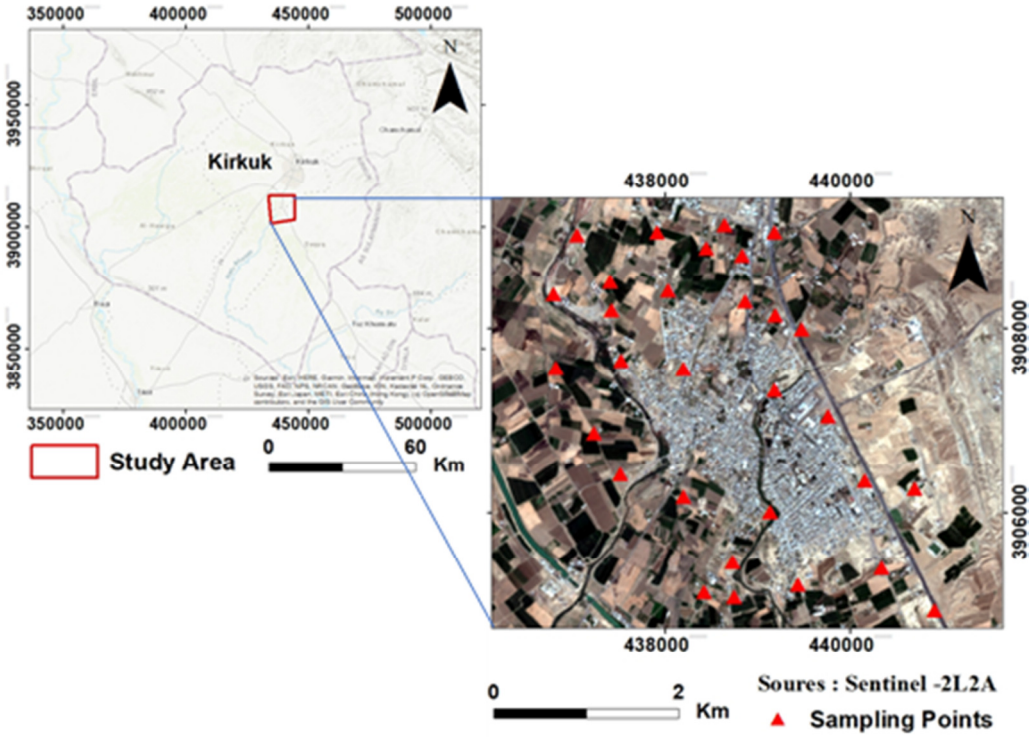

Fig. 1. Study area and sampling location.

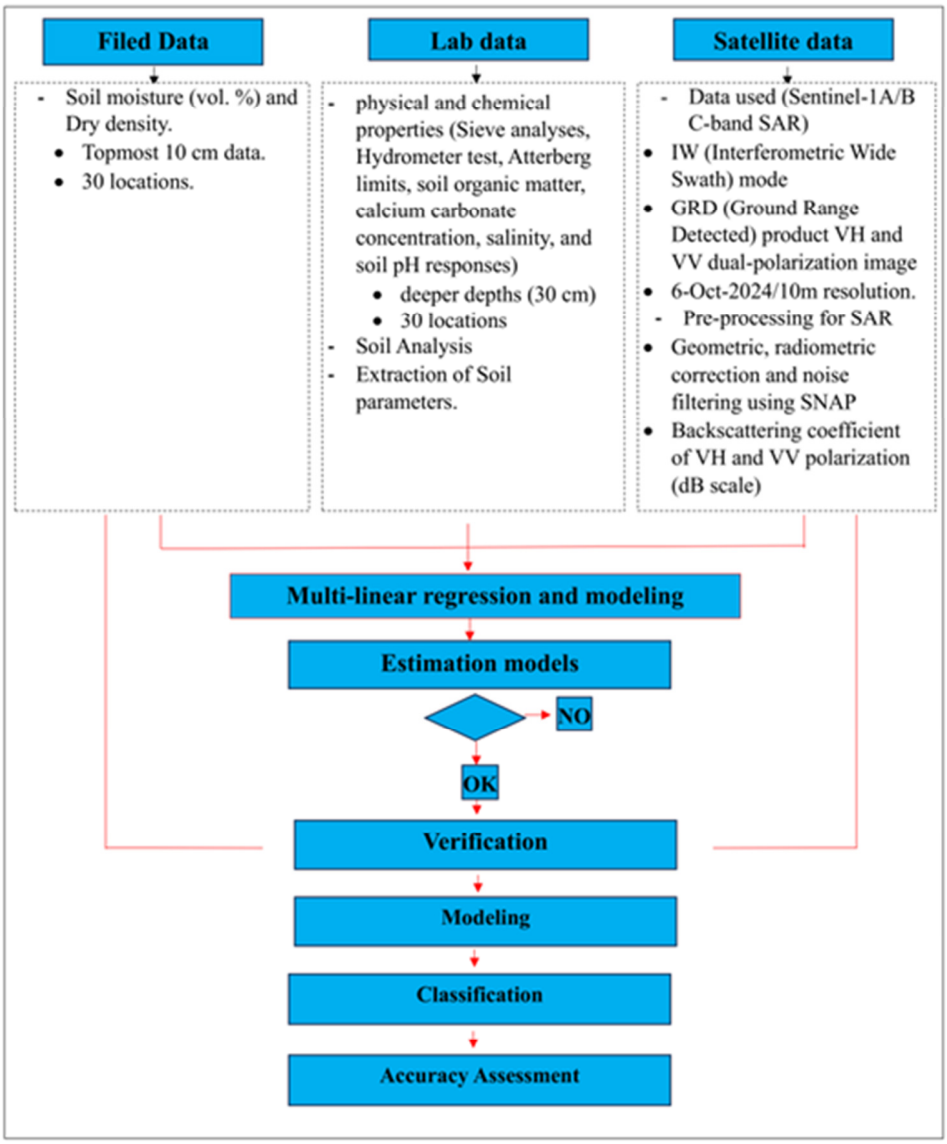

Fig. 2. Flowchart of the methodology.

B. Lab Data

All samples underwent drying, sieving, and pulverization before the physical and chemical characteristics could be measured. Several laboratory assessments the measured soil moisture, texture, organic matter content, calcium carbonate concentration, salinity, and soil pH values. A Casagrande device measured the Liquid Limit (*LL*) and Plastic Limit (*PL*) to determine the Plasticity Index (*PI*), as the difference between the *LL* and *PL*. The results are presented in Table I. To determine the soil texture, sieve analysis was conducted to classify the particles in the samples into gravel, sand, silt, and clay fractions. In addition to determining the soil texture using sieve analysis in accordance with the ASTM D2487 standard [19], the soils were classified into the clay, silt, sand, and gravel categories. The technical procedures for the tests were conducted in accordance with ASTM D4318 specifications [20].

C. Satellite Images

The European Radar Observatory's initial component belongs to GMES satellite series, which the ESA designed through European Commission's (EC) financial backing [5]. The distribution of soil moisture has been mapped using Sentinel-1A data. Table II shows the specifications of Sentinel-1A data.

D. Preprocessing for the SAR Image

The SAR on both ERS-1 and ERS-2 satellites delivers detailed image acquisitions of the coastal areas along with ocean and polar ice, as well as the ground features. It works during all weather conditions and throughout day and night hours. It remains unaffected by the clouds and depends on the detection of the microwave reflection from/based on features of the Earth's surface [21].

TABLE I. SOIL SAMPLE PARAMETERS AND CLASSIFICATION BASED ON THE USCS

Point	Group name	Density kg/m^3	Moisture (%)	LL	PL	PI	G.S	Gravel (%)	Sand (%)	Silt (%)	Clay (%)	Group symbol
1	Silt	1.849	6.8	45.0	30.0	15.0	2.71	0.00	3.16	55.95	40.89	ML
2	Silt	1.652	15.2	49.0	33.5	15.5	2.70	0.14	5.02	52.82	42.02	ML
3	Silt	1.721	4.6	47.2	33.9	13.3	2.71	0.36	5.08	62.09	32.47	ML
4	Silt	1.505	14.7	39.6	27.6	12.0	2.72	0.52	5.26	54.43	39.79	ML
5	Silt	1.747	6.6	42.5	31.5	11.0	2.70	0.20	6.32	57.69	35.79	ML
6	Silt with sand	1.582	3.6	35.5	26.5	9.0	2.69	0.60	21.46	54.25	23.69	ML
7	Silty sand	1.538	2.9	-	-	-	2.66	0.00	65.06	29.84	5.1.0	SM
8	Silty sand with gravel	1.675	1.7	-	-	-	2.65	23.22	57.04	16.08	3.66	SM
9	Silty gravel with sand	1.821	3.4	-	-	-	2.67	41.0	17.88	33.49	7.63	GM
10	Silty sand with gravel	1.851	2.2	-	-	-	2.65	19.6	39.16	33.59	7.65	SM
11	Silty clay	1.714	11	15.0	9.00	6.0	2.76	0.24	9.42	46.84	43.5	ML-CL
12	Silty clay	1.979	8.2	15.5	10.5	5.0	2.78	6.66	7.56	41.09	44.69	ML-CL
13	Silty clay	1.612	10.5	22.1	16.6	5.5	2.76	0.06	13.5	43.24	43.2	ML-CL
14	Silt with sand	1.403	2.8	32.0	24.0	8.0	2.69	0.40	16.5	58.8	24.3	ML
15	Silty clay	1.585	4.8	17.5	11.5	6.0	2.75	0.00	11.0	46.14	42.86	ML-CL
16	Silt with sand	1.620	2.2	37.5	28.5	9.0	2.7	0.00	24.69	49.48	25.83	ML
17	Silt with sand	1.701	2.9	34.8	25.5	9.3	2.68	0.10	26.1	52.6	21.20	ML
18	Silt with sand	1.831	5.0	40.0	34.0	6.0	2.70	0.00	24.5	52.55	22.95	ML
19	Sandy silt	1.533	2.3	45.5	36.5	9.0	2.67	0.06	34.26	48.31	17.37	ML
20	Lean clay with sand	1.632	4.5	22.0	13.0	9.0	2.72	0.04	21.0	36.66	42.30	CL
21	Sandy silt	2.005	3.3	36.0	30.0	6.0	2.73	0.32	37.4	43.35	18.93	ML
22	Silt	1.670	4.7	42.0	27.7	14.3	2.70	0.38	8.04	63.75	27.83	ML
23	Silt with sand	1.868	3.1	32.0	25.0	7.0	2.70	0.32	17.32	57.33	25.03	ML
24	Silt	2.070	3.9	38.0	27.0	11	2.71	0.70	12.32	58.83	28.15	ML
25	Silt	1.863	4.1	45.0	33.0	12	2.75	0.07	10.2	60.53	29.20	ML
26	Silt with sand	1.660	6.4	44.0	35.0	9.0	2.73	0.02	15.1	54.29	30.59	ML
27	Sandy silt	1.455	4.9	37.0	26.0	11	2.72	0.36	37.0	41.13	21.51	ML
28	Silt with sand	1.687	4.5	43.0	30.5	12.5	2.71	0.06	17.9	58.72	23.32	ML
29	Sandy silt	1.716	4.1	38.0	27.0	11	2.65	5.62	34.88	46.11	13.39	ML
30	Silt	1.870	4.0	41.0	32.0	9.0	2.70	0.32	12.12	59.22	28.34	ML

TABLE II. PROPERTIES OF THE USED SENTINEL-1A DATA.

Specifications	Sentinel-1A data
Sensing time	6-Oct-24
Orbit direction	Descending
Acquisition mode	IW
Radar frequency	C-band (5.4 GHz)
Polarization	VV-VH
Product type	GRD
Resolution mode	10 m

The image enhancement processes improve the image quality to facilitate better visualization and analysis from both human and machine perspectives [22]. Post-processing was conducted on each image, including the removal of thermal noise, radiometric calibration, geometric correction, and speckle filtering. The workflow scheme of the image preprocessing is illustrated in Figure 3.

E. Classification Methods

The satellite images and other image classification techniques consist of two methods: supervised and unsupervised. In a supervised technique, the operator describes the areas where diverse land cover is present. In the unsupervised technique, the computer develops spectral signatures by mathematical data clustering in the multidimensional feature space. Because of their effectiveness with complex, nonlinear relationships within multidimensional data, the KNN, RF, and MD algorithms were chosen. KNN was selected since it is straightforward and works with local groupings, RF was included due to its strength, high accuracy, and abilities with multifarious features, and MD was added for being efficient and designed for classes that are well divided in the distribution. The algorithms were examined using multiple linear regression, various accuracy statistics, and were compared against readings from field experiments to check their ability to predict.

a) K-Nearest Neighbor

KNN is a non-parametric method that has been used in statistical applications since the 1970s [23]. It is widely employed to identify a collection of K samples in the calibration dataset that are closest to unknown samples, frequently using distance functions. The labels of the unknown samples are ascertained by computing the average of the response variables, namely the class characteristics of the K closest neighbors [24]. Consequently, K is crucial to the success of KNN for this classifier, serving as the primary tuning parameter. However, the K parameter was determined by a bootstrap procedure [25].

b) K-Dimensional Tree

The KD-Tree is a method for space segmentation, and its workflow is divided into two phases: the offline phase and the online phase. Throughout the offline phase, an index (tree) is constructed to facilitate the query responses in the online segment. Furthermore, in the first phase, it/the tree partitions a

space into rectangular cells utilizing a splitting algorithm. In the conventional split, the dimension for partitioning is selected according to the highest dispersion along a dimension in the dataset. In the midway split, the splitting hyperplane divides the longest side of the cell that passes over its center [26].

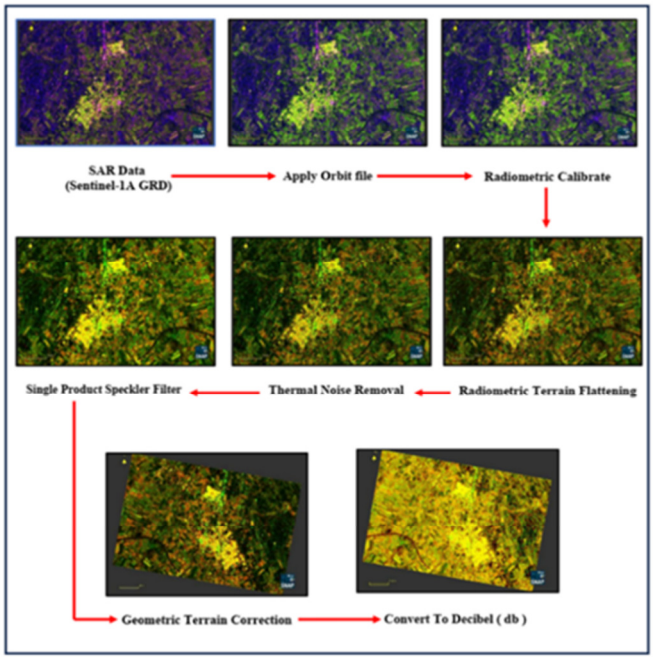

Fig. 3. Workflow scheme of the image preprocessing.

c) Random Forests

The RF is an ensemble classification technique derived from the shooting method [27]. It utilizes several independent Classification and Regression Trees (CARTs) as the foundational classifiers $\{h(x, \theta_k), k = 1\}$, where h denotes the RF classifier, x represents the input vector, and (θ_k) signifies the independent identically distributed random vectors used to generate each CART. In labeling, each tree casts a single vote for the most prevalent class on each input instance, and the final label is established via a majority vote among the trees. RF assesses the feature significance utilizing out-of-bag data using the permutation importance metric [23]. The predictions can be calculated by:

$$\hat{y} = \frac{1}{n}\sum_{i=1}^{n} y_i \quad (1)$$

where $\hat{y}$ represents the expected value, while y_1, y_2, ..., n are the predicted values from separate decision trees.

d) Minimum Distance Classification

The MD technique is efficient and widely used because of its mathematical simplicity, necessitating just the mean vectors for each band derived from the training data [28]. It is a nonparametric classifier that uses the mean vectors of each end member and computes the Euclidean distance from each unknown pixel to the mean vector of each class [29]. All the pixels are categorized into the closest class unless a standard deviation or distance threshold is established. In such illustrations, some pixels may remain unclassified if they fail to satisfy the set requirements.

F. Multiple Linear Regression Analysis

Multiple linear regression analysis is conducted to ascertain the correlations between two or more variables, exhibiting the basis of these relationships, and to facilitate predictions about the subject based on these relationships. The objective is to signify the dependent variable as a linear function of the independent variables [12]. The multiple linear regression outputs are determined using [30]:

$$Y = B_0 + B_1X_1 + \quad (2)$$

where Y is a dependent variable, B_0 is the intercept, X is the independent variable, and ε is the error term, as outlined in Table III.

TABLE III. MULTIPLE LINEAR REGRESSION ANALYSIS OF PHYSICAL PROPERTIES

Equations	R^2
$sand = 99.81 + (-1.016 \times silt) + (-1.035 \times clay) + 0.049LL$	0.93
$sand = 96.22 + (-0.98 \times silt) + 94.58 \times org(wt) + 0.001TDS - PPM + (-1.09 \times clay)$	0.94
$silt = 100.926 + (-0.896 \times sand) + (-0.964 \times GYP) + (-1.022 \times clay)$	0.97
$clay = 96.656 + (-0.866 \times sand) + (-0839GYP) + (-0.945 \times silt)$	0.97
$clay = 94.442 + 0.04 \times PL + (-0.869 \times sand) + (-0.949 \times silt)$	0.96
$LL = -26.914 + 0.078 \times sand + 1.125 \times silt$	0.59
$LL = 722.054 + (-0.284 \times sand) + 0.561 \times silt + 265.634 \times GYP + 0.22 \times clay$	0.73
$PL = -26.556 + 0.199 \times sand + 0.914 \times silt$	0.60

G. Accuracy Assessment

The two predominant measurements are the Overall Accuracy (OA) and the Kappa statistic (Table IV. The kappa statistic has become less prevalent in the measurement of the categorization accuracy in remote sensing. A limitation of just using the OA measure is that it fails to indicate the distinct performance of each class. Moreover, if the input datasets (training samples) are significantly unbalanced, the overall OA metric may be ambiguous, as few classes may be ineffectively recognized.

IV. RESULTS AND DISCUSSION

A. Backscatter and Model Generation

The USCS simplified the identification of several soil classifications. It serves as the foundation for soil classification because it offers appropriate criteria for the construction materials. USCS categorizes soils into two groups: coarse-grained soils, which include sand and gravel with 50% or less of the material passing through the No. 200 sieve, and fine-grained soils, which consist of materials where more than 50% passes through the No. 200 sieve. The subcategories are silt with sand (33.63%), silt (31.05%), sandy silt (15.92%), silty clay (11.82%), lean clay with sand (4.13%), silty sand with gravel (2.05%), silty sand (0.76%), and silty gravel with sand (0.64%). The percentages were derived via the KD-Tree technique. While in the KNN technique, the subcategories are

silt and sand (33.62%), silt (31.05%), sandy silt (15.92%), silty clay (11.82%), lean clay and sand (4.13%), silty sand with gravel (2.05%), silty sand (0.76%), and silty gravel with sand (0.64%). These soil classifications are illustrated in Figure 5. The RF method is one of the most effective classifiers and has been extensively documented in remote sensing works. It has been used for several purposes, including the soil texture study and classification, as well as the land usage for agricultural activity.

Figure 4 shows the soil category map of the study area derived from the modified USCS of the SAR parameters via various classifier algorithms, namely KD-Tree, KNN, RF, and MD. In the RF technique, the subdivisions are silt with sand (30.26%), silt (34.81%), sandy silt (12.35%), silty clay (12.32%), lean clay with sand (3.73%), silty sand with gravel (3.41%), silty sand (1.63%), and silty gravel with sand (1.49%). While, for the MD technique, the subcategories are silt with sand (4.49%), silt (29.39%), sandy silt (4.24%), silty clay (9.25%), lean clay with sand (5.13%), silty sand with gravel (4.87%), silty sand (17.65%), and silty gravel with sand (24.97%). Thirty soil samples were simulated on the map, showing the fractions of each type. The simulation results from this work revealed that the MD yielded more favorable findings than the other three methods (KD-tree, KNN, and RF). However, the findings from the MD method differ from those of the first three methods.

The results obtained from the algorithmic classification techniques were very close to the classifying models of the fieldwork, as depicted in Figure 6. The classifications were silt with sand, followed by silt, followed by sandy silt, followed by silty clay, followed by lean clay with sand, followed by silty sand with gravel, followed by silty sand, and finally followed by and silty gravel with sand. Table IV displays the accuracy assessment of the considered classification methods. The MD technique had different percentages extracted from it, which were silt, followed by silty gravel with sand, followed by silty clay, followed by silty sand with gravel, followed by lean clay with sand, followed by silt with sand, and followed by sandy silt, as shown in Table IV. The USCS classification of 30 samples revealed that there are nine samples of silt, eight samples of silt with sand, four samples of silty clay and sandy silt, two samples of silty sand with gravel, and two samples of silty sand with gravel and lean clay with sand, as portrayed in Table I.

The results indicate that the study area is located within the alluvial fan deposits [18]. The locations exhibiting elevated percentages of gravel and sand are presumed to have originated from regions closer to the Khasa-Su River, and these samples did not indicate any restrictions regarding the soil texture. Subsequently, the USCS results revealed that most of the samples taken from the field were composed of silt, followed by silt with sand, silty clay, and sandy followed by silt silty sand with gravel, finally followed by silty sand with gravel and lean clay with sand, as presented in Table I.

The findings of the accuracy assessment show that KD-Tree, KNN, and RF, produced favorable outcomes across most categories, exhibiting a close alignment in values and reflecting their classification accuracy.

In contrast, the MD technique had a worse performance compared to the preceding methods. Conversely, the fourth approach was poorly performed in comparison to the previous techniques. The study has practical significance in identifying the soil in Kirkuk city [31].

B. Soil Classification

The gravel proportion was minimal, and it could be neglected, except for four sites, which ranged between 6% and 41%. The sand percentage ranged between 3% and 39%, except for two sites that showed a high proportion between 57%-65%. The silt fraction was high in most of the samples, which ranged between 30% and 63%, except for one site, where it was below 20%, while the clay contents were between 3% and 40%. However, it was observed that silt represented the highest volume percentage, followed by clay and sand, while the gravel was present in negligible amounts, appearing only in certain locations, as shown in Figures 4 and 5, and Table I.

C. Multiple Linear Regression Analysis

The multiple linear regression analysis results indicated positive moderate correlations between the soil characteristics, ranging from 0.59 to 0.93, as evidenced in Figure 6 and Table III.

TABLE IV. ACCURACY ASSESSMENT FOR THE CLASSIFICATIONS

Classes	**MD classification**		**KD-Tree**		**KNN**		**RF**	
	User acc.%	Producer acc. %	User acc.%	Producer acc. %	User acc.%	Producer acc. %	User acc.%	Producer acc. %
Silt	72.00	54.55	88.46	80.70	87.6	83.50	92.31	81.03
Silty sand	91.43	72.73	80.00	78.57	81.0	79.10	87.50	79.55
Lean clay, sand	58.82	66.67	73.33	92.11	74.2	89.19	80.00	94.74
Silt, sand	86.36	100.0	85.71	79.63	85.1	77.78	85.71	80.77
Silty clay	78.79	92.86	83.87	81.25	82.6	76.47	83.87	74.29
Silty gravel, sand	93.07	87.85	86.49	96.97	88.5	96.97	86.49	96.97
Sandy silt	84.62	91.67	82.61	82.61	83. 1	80.85	82.61	86.36
Silty sand, gravel	61.29	86.36	82.05	84.21	82.9	88.89	82.05	88.89
OA	0.814		0.92		0.91		0.93	
Kappa	0.77		0.91		0.89		0.92	

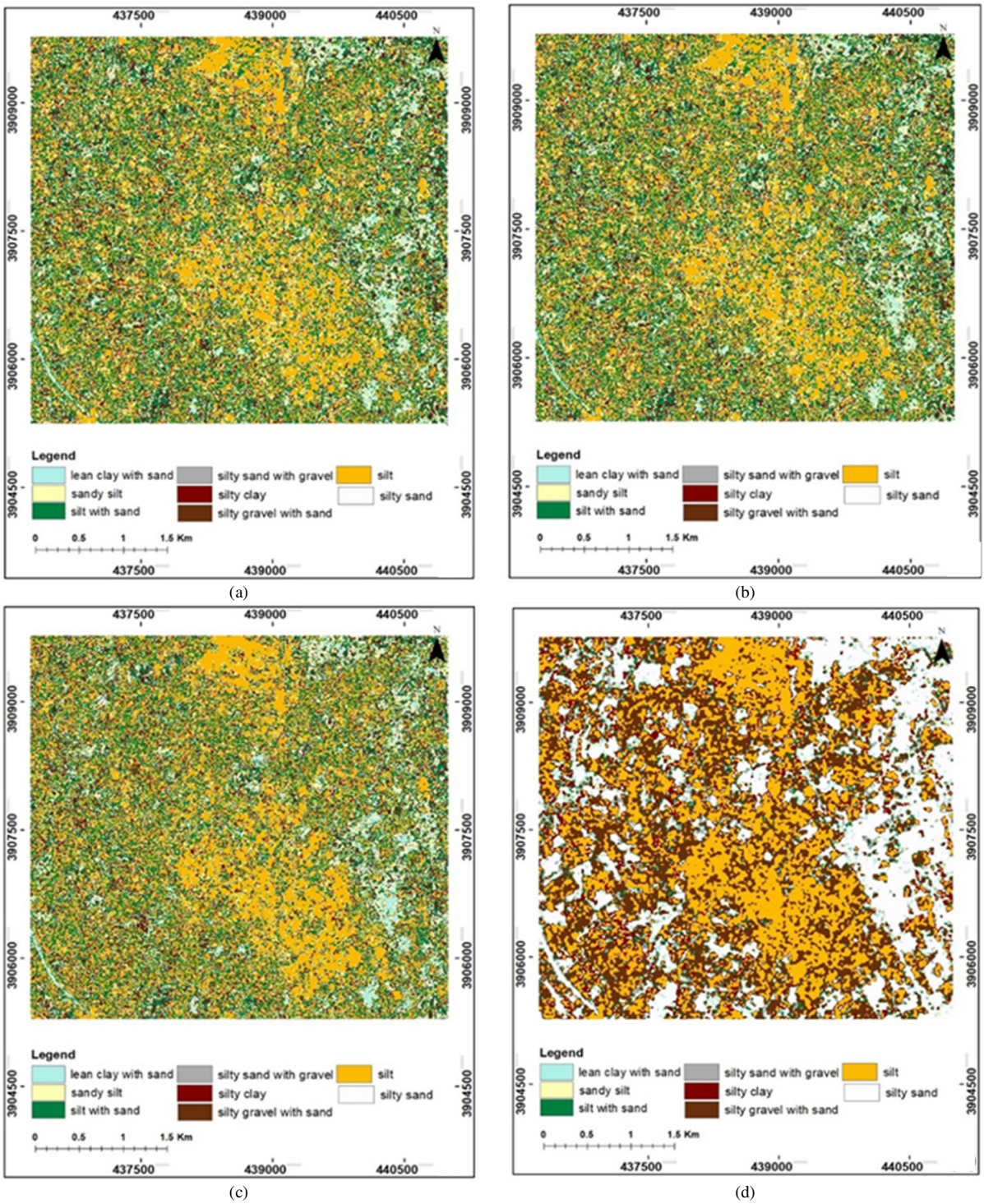

Fig. 4. Soil classification maps of the study area simulated according to the USCS standard of SAR parameters utilizing: (a) KD-tree, (b) KNN, (c) RF, and (d) MD.

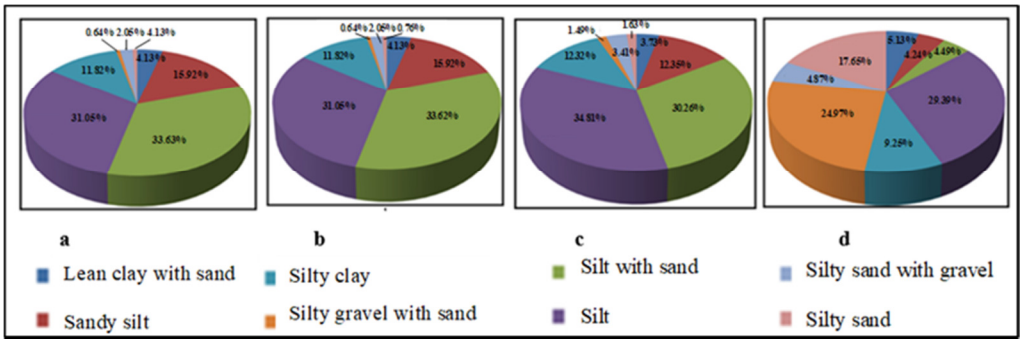

Fig. 5. Percentage of soil classifications illustrating the ratio of: (a) KD-tree, (b) KNN, (c) RF, and (d) MD.

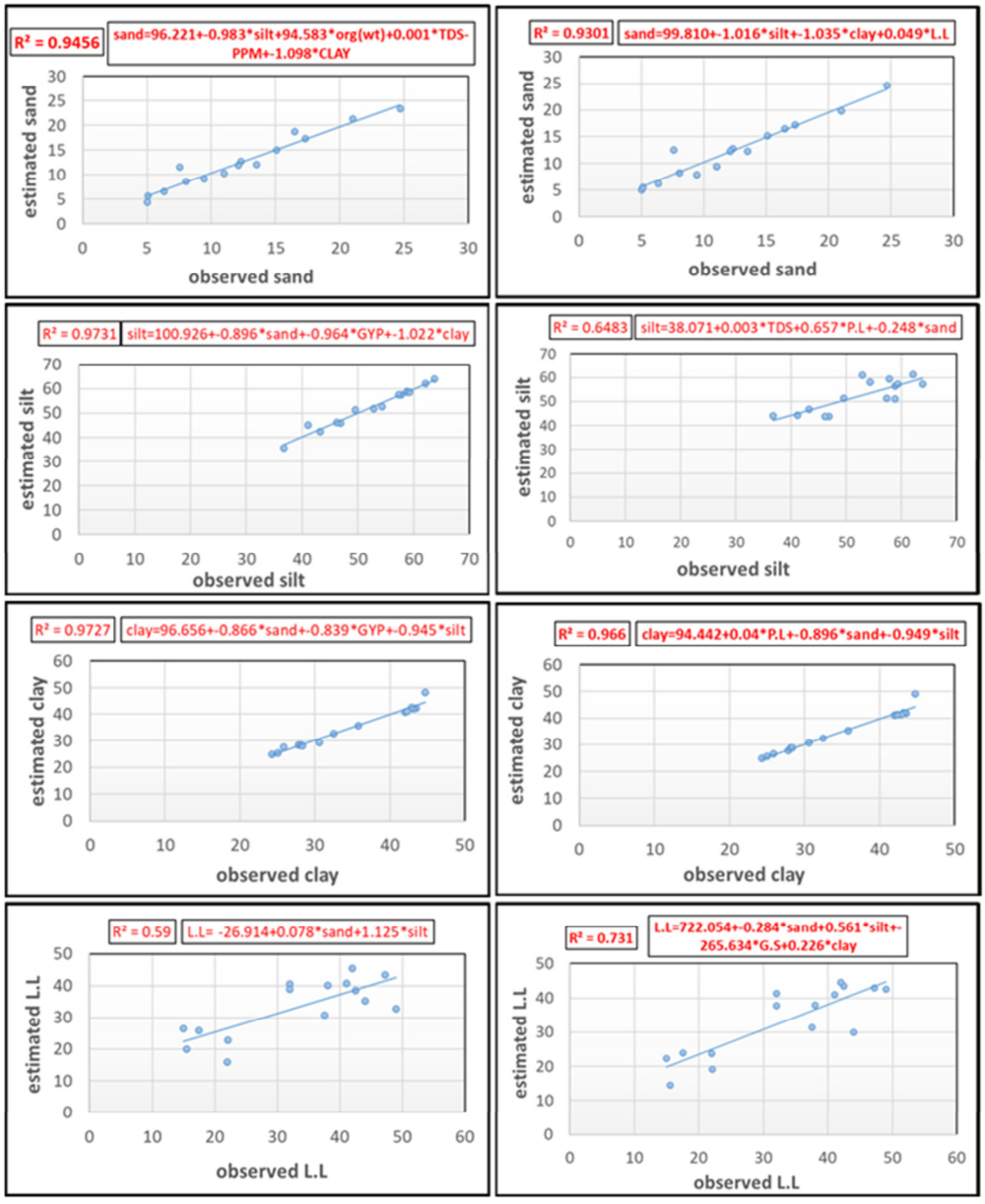

Fig. 6. Multiple regression analysis of the physical properties.

V. CONCLUSION

The findings of the present work demonstrated that the Unified Soil Classification System (USCS) effectively identified eight distinct subcategories of soil. The soil samples were carefully classified according to their grain size. This study reveals that the classification techniques based on field algorithms and operating through C-band Synthetic Aperture Radar (SAR) data demonstrate effective soil property prediction abilities. Through soil tests, the main type of soil found at most locations is silty, and the second is clayey or sandy, except that gravel is minuscule at few sites. These findings suggest that the soil has a fine texture, which may affect the way it holds the water and the nutrients. The K-Dimensional Tree (KD-Tree), K-Nearest Neighbor (KNN), and Random Forest (RF) algorithms demonstrated superior performance compared to the Minimum Distance (MD), obtaining greater accuracy in the classification process. Moderate to strong positive correlations (0.59-0.93) were found by multiple linear regression analysis, implying that the adjustments in one soil parameter tend to predict the changes in others. Such results demonstrate that different soil properties work together and confirm the importance of using regression models for judging the soil quality. Examining the soil properties and observing their interrelations can help manage the land at a specific site. These models show great potential for soil texture categorization via SAR imaging. Nonetheless, their true potential can be fully realized through an evaluation across diverse geographic regions with varying climatic conditions. This technique can be applied in many semi-arid and data-scarce regions, enabling a rapid soil assessment using SAR data combined with machine learning methods. It makes things easier by cutting down on fieldwork and helping with precise agriculture and land care. However, challenges remain in applying these models across diverse terrain types and with different sensor types. In future, further research can be performed entailing multiple time periods and comparative analyses across different regions to establish a generalized technique.

REFERENCES

[1] H. Yu, B. Kong, G. Wang, R. Du, and G. Qie, "Prediction of soil properties using a hyperspectral remote sensing method," *Archives of Agronomy and Soil Science*, vol. 64, no. 4, pp. 546–559, Mar. 2018, https://doi.org/10.1080/03650340.2017.1359416.

[2] N. Baghdadi *et al.*, "A Potential Use for the C-Band Polarimetric SAR Parameters to Characterize the Soil Surface Over Bare Agriculture Fields," *IEEE Transactions on Geoscience and Remote Sensing*, vol. 50, no. 10, pp. 3844–3858, Oct. 2012, https://doi.org/10.1109/TGRS.2012.2185934.

[3] B. M. Das and K. Sobhan, *Principles of geotechnical engineering*, 9th ed. Boston, MA: Cengage Learning, 2018.

[4] R. Pal and N. Jana, "Predicting the spatial patterns of soil erosion hazard using RUSLE and frequency ratio in the Silabati River Basin eastern India," *DYSONA - Applied Science*, vol. 6, no. 2, Jul. 2025, https://doi.org/10.30493/das.2025.510627.

[5] M. T. Esetlili and Y. Kurucu, "Determination of Main Soil Properties Using Synthetic Aperture Radar," *Fresenius Environmental Bulletin*, vol. 25, no. 1, pp. 23–36, 2016.

[6] A. H. Ameen, A. A. Hafssa, H. J. Jumaah, and Q. H. Eapak, "Hospital site selection using AHP-based GIS in Tikrit City, Iraq," in *9th Advanced Engineering Days*, Tabriz, Iran, Jul. 2024, vol. 9, pp. 147–149.

[7] L. Tao, J. Li, J. Jiang, S. He, Q. Cai, and X. Chen, "Evaluation of radar backscattering models using L- and C-band synthetic aperture radar data," *Journal of Applied Remote Sensing*, vol. 9, no. 1, Dec. 2015, Art. no. 094091, https://doi.org/10.1117/1.JRS.9.094091.

[8] M. H. Ameen, M. Azmi, and H. J. Jumaah, "Evaluating Exposure to Road Traffic Air and Noise Pollution: A Comprehensive Review of Assessment Methods," *Tikrit Journal of Engineering Sciences*, vol. 32, no. 2, pp. 1–19, May 2025, https://doi.org/10.25130/tjes.32.2.9.

[9] F. Bovenga, "Special Issue 'Synthetic Aperture Radar (SAR) Techniques and Applications,'" *Sensors*, vol. 20, no. 7, Mar. 2020, Art. no. 1851, https://doi.org/10.3390/s20071851.

[10] H. J. Jumaah, B. Kalantar, N. Ueda, O. S. Sani, Q. M. Ajaj, and S. J. Jumaah, "The Effect of War on Land Use Dynamics in Mosul Iraq Using Remote Sensing and GIS Techniques," in *2021 IEEE International Geoscience and Remote Sensing Symposium IGARSS*, Brussels, Belgium, Jul. 2021, pp. 6476–6479, https://doi.org/10.1109/IGARSS47720.2021.9553165.

[11] G. K. Uyanık and N. Güler, "A Study on Multiple Linear Regression Analysis," *Procedia - Social and Behavioral Sciences*, vol. 106, pp. 234–240, Dec. 2013, https://doi.org/10.1016/j.sbspro.2013.12.027.

[12] N. R. Smalheiser, *Correlation and Other Concepts You Should Know*. Data Literacy, Elsevier, 2017.

[13] B. M. Das, *Soil mechanics laboratory manual*, 6th ed. New York, New York State: Oxford University Press, 2002.

[14] C. A. Ali, M. A. Shareef, and Q. A. M. Al Nuaimy, "Estimating Soil Parameters Using C Band Synthetic Aperture Radar in Laylan, Iraq," *Ecological Engineering & Environmental Technology*, vol. 25, no. 9, pp. 26–36, Sep. 2024, https://doi.org/10.12912/27197050/189889.

[15] V. L. Mironov, P. P. Bobrov, S. V. Fomin, and A. Yu. Karavaiskii, "Generalized refractive mixing dielectric model of moist soils considering ionic relaxation of soil water," *Russian Physics Journal*, vol. 56, no. 3, pp. 319–324, Aug. 2013, https://doi.org/10.1007/s11182-013-0034-4.

[16] P. A. Mohammed, Q. A. M. Al Nuaimy, and M. A. Shareef, "Analyzing Soil Physical Properties in Kirkuk City, Iraq, utilizing a Geographic Information System – Based Inverse Distance - Weighted Technique," *Ecological Engineering & Environmental Technology*, vol. 25, no. 11, pp. 118–133, Nov. 2024, https://doi.org/10.12912/27197050/192346.

[17] H. J. Jumaah, M. H. Ameen, B. Kalantar, H. M. Rizeei, and S. J. Jumaah, "Air quality index prediction using IDW geostatistical technique and OLS-based GIS technique in Kuala Lumpur, Malaysia," *Geomatics, Natural Hazards and Risk*, vol. 10, no. 1, pp. 2185–2199, Jan. 2019, https://doi.org/10.1080/19475705.2019.1683084.

[18] S. Z. Jassim and J. C. Goff, *Geology of Iraq*. Prague: Moravian museum, 2006.

[19] *Standard Practice for Classification of Soils for Engineering Purposes (Unified Soil Classification System)*, ASTM D2487-17 ASTM International, West Conshohocken, Pennsylvania, 2017.

[20] *Standard Test Methods for Liquid Limit, Plastic Limit, and Plasticity Index of Soils*, ASTM D 4318-10, ASTM International, West Conshohocken, Pennsylvania, 2010.

[21] P. Kaushik and S. Jabin, "A Comparative study of Pre-processing Techniques of SAR Images," in *2018 4th International Conference on Computing Communication and Automation (ICCCA)*, Greater Noida, India, Dec. 2018, pp. 1–4, https://doi.org/10.1109/CCAA.2018.8777710.

[22] R. C. Gonzalez, R. E. Woods, and B. R. Masters, "Digital Image Processing, Third Edition," *Journal of Biomedical Optics*, vol. 14, no. 2, 2009, Art. no. 029901, https://doi.org/10.1117/1.3115362.

[23] P. Thanh Noi and M. Kappas, "Comparison of Random Forest, k-Nearest Neighbor, and Support Vector Machine Classifiers for Land Cover Classification Using Sentinel-2 Imagery," *Sensors*, vol. 18, no. 1, Dec. 2017, Art. no. 18, https://doi.org/10.3390/s18010018.

[24] Y. Akbulut, A. Sengur, Y. Guo, and F. Smarandache, "NS-k-NN: Neutrosophic Set-Based k-Nearest Neighbors Classifier," *Symmetry*, vol. 9, no. 9, Sep. 2017, Art. no. 179, https://doi.org/10.3390/sym9090179.

[25] Y. Qian, W. Zhou, J. Yan, W. Li, and L. Han, "Comparing Machine Learning Classifiers for Object-Based Land Cover Classification Using

Very High Resolution Imagery," *Remote Sensing*, vol. 7, no. 1, pp. 153–168, Dec. 2014, https://doi.org/10.3390/rs70100153.

[26] Y. Narasimhulu, A. Suthar, R. Pasunuri, and C. Venkaiah, "CKD-Tree: An Improved KD-Tree Construction Algorithm," in *ISIC 2021: International Semantic Intelligence Conference*, New Delhi, India, Feb. 2021, pp. 211–218.

[27] P. K. Shit, G. S. Bhunia, and R. Maiti, "Spatial analysis of soil properties using GIS based geostatistics models," *Modeling Earth Systems and Environment*, vol. 2, no. 2, Jun. 2016, Art. no. 107, https://doi.org/10.1007/s40808-016-0160-4.

[28] D. Lu and Q. Weng, "Spectral Mixture Analysis of the Urban Landscape in Indianapolis with Landsat ETM+ Imagery," *Photogrammetric Engineering & Remote Sensing*, vol. 70, no. 9, pp. 1053–1062, Sep. 2004, https://doi.org/10.14358/PERS.70.9.1053.

[29] M. Bouaziz, S. Eisold, and E. Guermazi, "Semiautomatic approach for land cover classification: a remote sensing study for arid climate in southeastern Tunisia," *Euro-Mediterranean Journal for Environmental Integration*, vol. 2, no. 1, Oct. 2017, Art. no. 24, https://doi.org/10.1007/s41207-017-0036-7.

[30] V. R. Srividhya and Kayarvizhy, "Streamlined Traffic Prognosis using Flexible Reservoir Sampling and Regression Methods," *Engineering, Technology & Applied Science Research*, vol. 15, no. 2, pp. 20827–20834, Apr. 2025, https://doi.org/10.48084/etasr.9889.

[31] A. H. Taqi, Q. A. M. Al Nuaimy, and G. A. Karem, "Study of the properties of soil in Kirkuk, IRAQ," *Journal of Radiation Research and Applied Sciences*, vol. 9, no. 3, pp. 259–265, Jul. 2016, https://doi.org/10.1016/j.jrras.2016.02.006.